JOURNAL OF MATERIALS SCIENCE 17 (1982) 1977–1987

Dynamics of flow of *c*-axis sapphire

D. M. KOTCHICK*, B. J. BUSOVNE†, R. E. TRESSLER
Materials Science and Engineering Department, The Pennsylvania State University, University Park, Pennsylvania, USA

D. J. BARBER
Physics Department, University of Essex, Wivenhoe Park, Essex, UK

The deformation dynamics in uniaxial tension of *c*-axis sapphire were investigated at temperatures from 1600 to 1850° C in constant strain-rate tests from 0.00007 min^{-1} to 0.0036 min^{-1}. The activation parameters are consistent with thermally-activated overcoming of the Peierls barrier as the rate-controlling process for flow. From SEM, TEM, and HVTEM examinations of deformed specimens it is deduced that the active slip plane is of the $\{\bar{4}\,2\,2\,3\}$-type. The dislocation structure suggests that the $\langle 0\,\bar{1}\,1\,0\rangle$ directions are the most likely slip directions.

1. Introduction

General plasticity of polycrystalline alumina can only take place when five independent slip systems are operative. Alumina, which is rhombohedral and highly anisotropic, deforms easily by basal slip, secondarily by prismatic slip, and with more difficulty on pyramidal plane(s). It is necessary to activate a pyramidal slip system to attain general plasticity since only four independent systems are available by basal and prismatic slip.

The extreme difficulty of initiating slip in *c*-axis of 0° sapphire was first noted in creep tests above 1600° C [1]. Subsequently, several macroscopic slip systems have been suggested by several investigators [2–4] from a variety of techniques, including etch-pit studies, TEM analysis and macroscopic slip traces. The $\{1\,0\,\bar{1}\,1\}\,1/3\,\langle 1\,0\,\bar{1}\,1\rangle$ has been the most frequently referenced, but slip on the $\{10\bar{1}2\}$ and $\{22\bar{4}3\}$ planes has also been suggested.

The rate-controlling mechanism for plastic deformation via pyramidal slip has not been convincingly determined. Heuer *et al.* [5] and Firestone and Heuer [6] proposed pure Nabarro climb deformation for 0° Czochralski-grown sapphire deformed from 1600 to 1800° C in tensile creep experiments at relatively low stresses (70 to 114 $MN\,m^{-2}$) and low strain rates (10^{-8} to 10^{-16} sec^{-1}). They based their conclusion on determination of a stress exponent, n of value three from a relation of the form $\dot{\epsilon} \propto \sigma^n$, where $\dot{\epsilon}$ is the strain rate and σ is the stress, and a fit of the apparent oxygen diffusion coefficients calculated assuming a Nabarro-climb mechanism.

Gooch and Groves [3] conducted tensile creep tests above 1600° C ($\dot{\epsilon}$ and σ of 10^{-6} sec^{-1} and 180 to 65 $MN\,m^{-2}$, respectively) on *c*-axis Tyco filaments (which contain microvoids of size about one micrometre) and found a stress exponent, n, of about six. They also found activation enthalpies with a marked stress dependence but did not speculate as to a rate-controlling mechanism.

Tressler and Barber [4] performed differential temperature and differential strain-rate tests on *c*-axis Tyco filaments and found a power-law dependence, with n values increasing from 8.5 to 1775° C to 12.4 to 1875° C. They also found a zero-stress activation enthalpy of approximately 80 kcal mol^{-1}.

Michael and Tressler [7] performed differential temperature and differential strain-rate tensile tests in the limited temperature range 1800 to 1850° C on pore-free *c*-axis filaments grown by the laser-heated floating-zone technique [8]. They

*Present address: AiResearch Mfg. Co., Torrance, California, USA.
†Present address: AC Division of General Motors, Flint, Michigan, USA.

0022–2461/82/071977–11$03.82/0

concluded that the most probable rate-controlling mechanism was the thermally-activated overcoming of the Peierls–Nabarro stress, based on the analysis of calculated activation parameters.

The purpose of this study was to perform deformation experiments on the virtually defect-free *c*-axis rods (grown by Haggerty [8]) over a wide range of temperatures and strain rates using differential temperature and differential strain-rate tests to define the apparent activation parameters for deformation of sapphire via the pyramidal slip system(s) more exhaustively than had previously been the case. From these results and TEM observations of the deformation substructure it was expected that a better assessment of the rate-controlling mechanism(s) for plastic deformation and more definitive identification of the operative slip system(s) could be made.

2. Experimental procedure

2.1. Material

Filaments used in this study were grown from a commercially-available sapphire boule by the crucibleless laser-heated floating-zone technique [8]. The single-crystal filaments were mechanically pulled at very slow rates using an oriented seed crystal to start the single crystal in the desired direction. Precise temperature control and pulling rate permitted control of the crystal dimensions.

Filaments were grown with crystallographic *c*-axis parallel to the filament axis. The filaments were nearly cylindrical, except for slight facetting on the prism planes, (see Fig. 1a). As-received crystals were approximately 20 cm long and 0.025 mm^2 in cross-section. Sample cross-sections were measured individually at 5 mm intervals along the hot-zone segment at 0°, 60°, and 120° rotations about the filament axis using a petrographic microscope with a calibrated eye-piece micrometer. The cross-sections for each rotation typically did not vary more than 0.3 mm along the 7 cm hot-zone length. An average of the three cross-section measurements was used to calculate a cross-sectional area estimated as a circle. The estimated error was less than 3% using micrographs of actual sample cross-sections (Fig. 1b) and an integrating planimeter to determine the actual area.

2.2. Testing procedure and equipment

Filaments were mounted in a stainless-steel hypodermic needle, as shown in Fig. 2. Each filament-end was slipped through a hypodermic needle casing and beaded in an oxygen-rich flame. The bead was then seated in the needle casing.

The mounted samples were placed into pivot bearing tensile testing grips designed by Tressler and Crane [9] (see Fig. 3). The pivot bearings enable very good alignment using the four adjustable screws which straddle the ball-bearing pivot. Each of the grips have a ball-bearing seat which allows rotation of the hypodermic needle casing to minimize bending moments. The grips were attached to water-cooled rams located inside a Centorr tungsten resistance vacuum furnace. The top ram was connected through a bellows to an Instron table-model testing machine. Only the centre of the filament passed through the heat shields to a 7 cm-long uniform hot zone.

Differential strain-rate and differential temperature tests were performed on all samples. Differential strain-rate tests were performed at constant

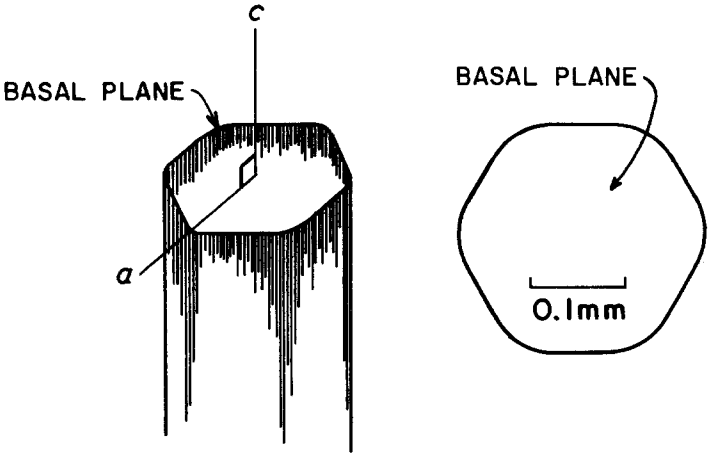

Figure 1 Schematic diagram of the *c*-axis filament morphology with a tracing of a micrograph of a filament cross-section.

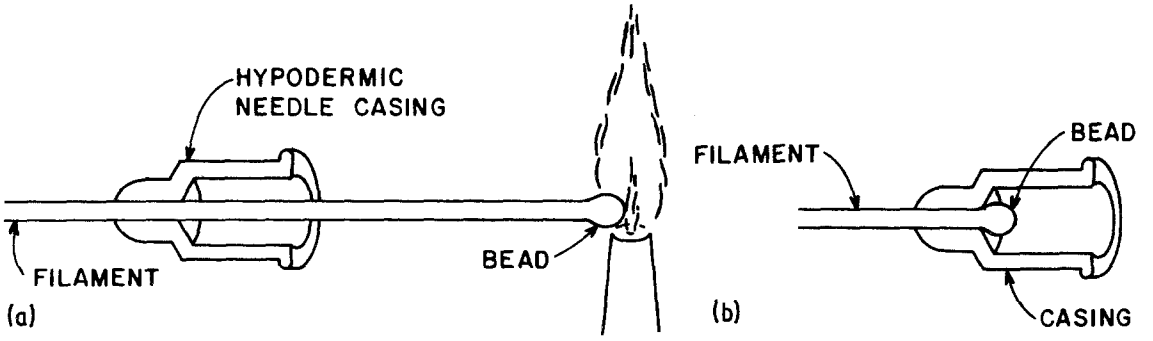

Figure 2 Preparation of the filaments for testing. (a) Beading the filament in an oxygen-rich flame and (b) bead seated in needle casing.

temperatures by changing the cross-head speed of the Instron machine (which took about 10 sec). Differential temperature tests were performed at constant strain rate, for which the cross-head was stopped during the change of temperature (which took about 30 sec). Differential strain-rate data and differential temperature data were used to calculate the activation parameters.

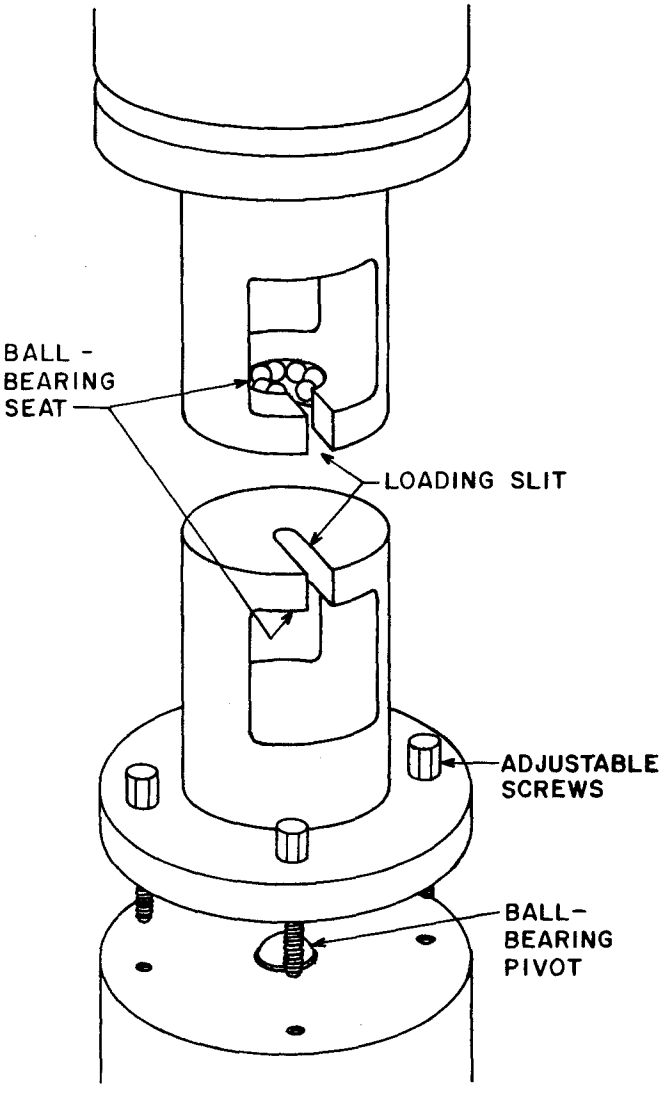

Figure 3 The pivot bearing grips used in tensile loading of the samples.

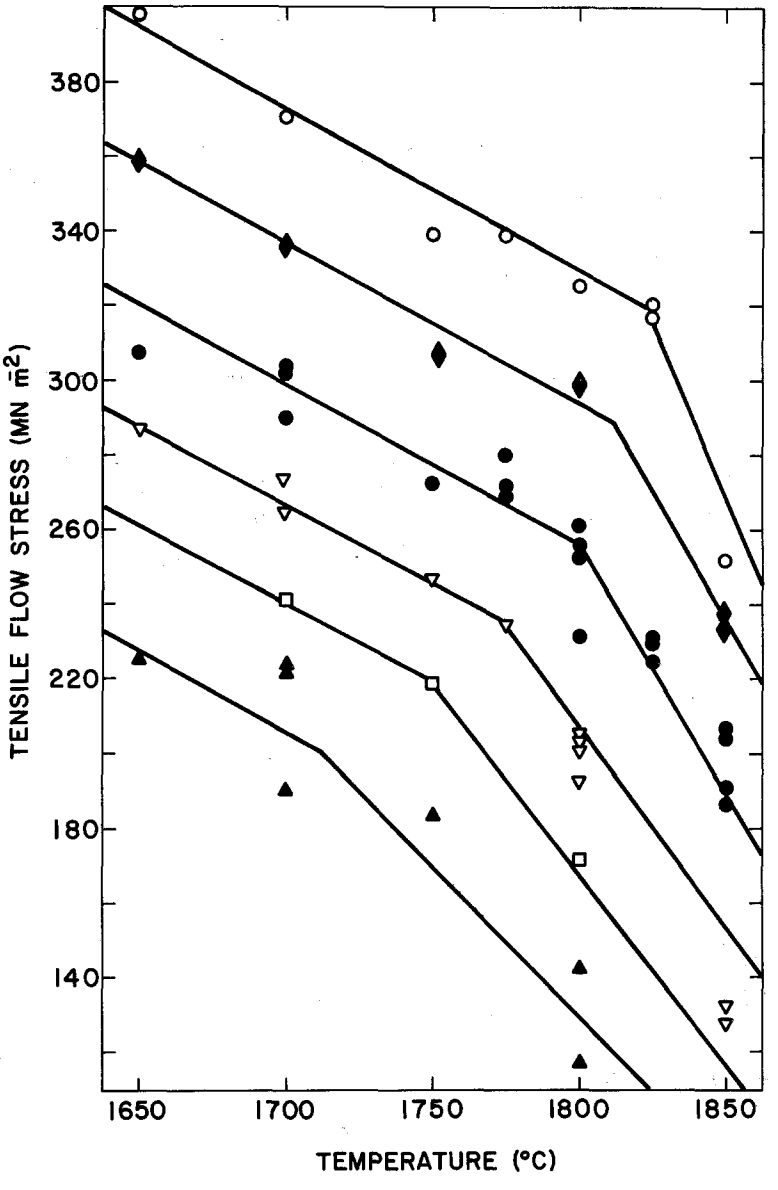

Figure 4 Tensile flow stress plotted against temperature for undoped *c*-axis sapphire. ○, 0.0036 min^{-1}; ♦, 0.0019 min^{-1}; ●, 0.000 73 min^{-1}; ▽, 0.000 36 min^{-1}; □, 0.000 19 min^{-1}; ▲, 0.000 07 min^{-1}.

2.3. Analysis of deformed samples

Samples were examined for accuracy of orientation by using a precison goniometer and transmission Laue X-ray diffraction pattern analysis. Slip-trace analysis was carried out using SEM microscopy coupled with Laue transmission X-ray orientation techniques to identify the macroscopic slip traces on the surface of the deformed crystals.

Emission spectroscopy was used to determine the purity in both deformed and undeformed crystals. The quantitative spectrographic analysis indicate that the impurity levels in the deformed samples were $SiO_2 \sim 0.02$ wt%, $Cr_2O_3 < 0.05$ wt%, $TiO_2 < 0.01$ wt%, $CaO < 0.03$ wt% and $FeO < 0.01$ wt%. These quantities are probably higher than the actual impurity contents in the bulk of the samples since the high surface-to-volume ratio and the thermal history of the filaments suggest probable surface contamination. Additionally, the filament growth technique zone-refines the starting material which had impurity levels of less than 0.01 wt% of SiO_2, TiO_2 and Cr_2O_3. The chromium content of the filaments was probably less than that indicated by the analysis because the samples were crushed for analysis using a chromium-doped alumina mortar and pestle.

Foils with prism plane orientation were prepared for TEM examination by diamond-polishing to a thickness of 0.51 mm through 30, 15, 6 and 1 μm diamond sizes on each side. Samples were ion-milled

and coated with carbon before TEM examination at 100 kV (using Phillips EM 300 machine) and HVTEM examination at 1 MV (using an AEI EM7 machine).

3. Results and discussion

3.1. Mechanical test results

The stress–strain curves were similar to those reported previously [7] containing an elastic region, an upper yield stress, and a constant flow stress for each strain-rate tested, independent of elongation.

Differential temperature tests were run at constant strain rate where a temperature change of 25° C took about 30 sec and the cross-head was stopped during the temperature change. Both the differential strain-rate and differential temperature tests were commonly run on individual samples.

The upper yield stress values plotted as a function of temperature are scattered. This scatter is probably due to the upper yield stress being a function of initial mobile dislocation density, which is dependent on the thermal and stress history of the samples, which were not identical in all cases. The in-grown dislocation density of as-received samples was very low ($\simeq 1.0 \times 10^6$ m^{-2} from etch-pit analysis).

The flow stress was independent of strain for all temperatures and strain rates investigated. Fig. 4 is a composite of flow stresses collected in differential temperature and differential strain-rate tests for six strain rates. The constant strain-rate curves suggest a break in the flow behaviour at high temperatures. The constant strain-rate curves were used to calculate the activation enthalpies and activation volumes.

3.2. Activation analysis

The flow behaviour of sapphire has generally been fitted to two types of equations. For dislocation barriers such as the overcoming of the Peierls–Nabarro stress, flow data have been fit to an equation in which the strain rate is exponentially dependent on stress:

$$\dot{\epsilon} = \nu \exp(-H(\sigma)/RT), \quad (1)$$

where $\dot{\epsilon}$ is the strain rate, ν is a constant, $H(\sigma)$ is the stress-dependent activation enthalpy, R is the gas constant and T is the absolute temperature. Generally, such processes have been associated with relatively low temperatures from 900 to 1700° C [10–12]. For dislocation processes such as diffusion-controlled climb, the flow results have been fitted to an equation in which the strain rate is dependent on the stress to some power:

$$\dot{\epsilon} = (A/T)\sigma^n \exp(-H_0/RT), \quad (2)$$

where A and n are constants and H_0 is the activation enthalpy which is relatively independent of stress [13]. The flow data was analysed using these equations to determine the activation parameters.

Stress exponents were calculated from flow stresses collected in differential strain-rate experiments from

$$n = \frac{\delta \ln \dot{\epsilon}}{\delta \ln \sigma} \sim \frac{\Delta \ln \dot{\epsilon}}{\Delta \ln \sigma}, \quad (3)$$

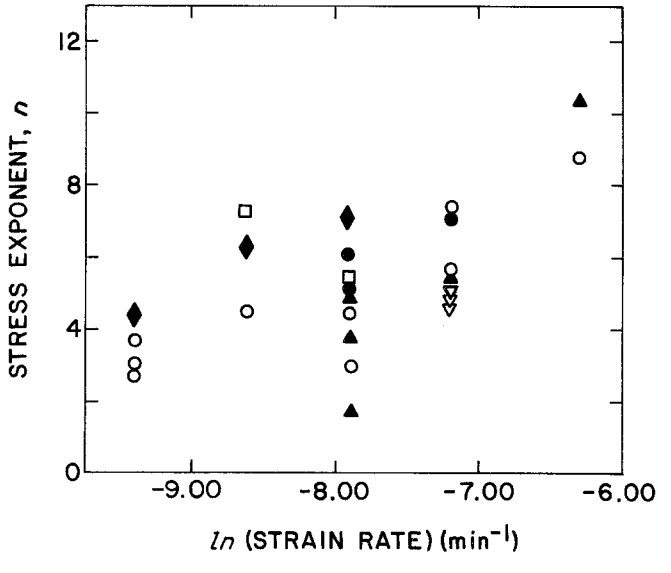

Figure 5 Stress exponent plotted against ln (strain rate) at constant temperatures for undoped *c*-axis sapphire. ▲, 1850° C; ▽, 1825° C; ○, 1800° C; ●, 1775° C; ♦, 1750° C; □, 1700° C.

assuming a deformation equation of the form of Equation 2. The activation volume can be calculated assuming an expression of the form

$$\dot{\epsilon} = \exp\left[-(H_0 - V^*\sigma_{\text{flow}})/RT\right], \quad (4)$$

where $\dot{\epsilon}$ and σ_{flow} are the shear strain-rate and shear flow-stress, respectively, and V^* is the activation volume. V^* can then be expressed [4] by

$$V^* = RT\frac{\delta \ln \dot{\epsilon}}{\delta \tau} \sim RT\left(\frac{\Delta \ln \dot{\epsilon}}{\Delta \sigma}\right)_T [1/(\cos\theta \cos\phi)]. \quad (5)$$

The activation enthalpy can be calculated from

$$\frac{\Delta H}{RT^2} = \left(\frac{\delta \ln \dot{\epsilon}}{\delta \sigma}\right)_T \left(\frac{\delta \sigma}{\delta T}\right)_{\dot{\epsilon}} \sim \left(\frac{\Delta \ln \dot{\epsilon}}{\Delta \sigma}\right)_T \left(\frac{\Delta \sigma}{\Delta T}\right)_{\dot{\epsilon}}, \quad (6)$$

using data from differential strain-rate and differential temperature tests, when, as in this study, the applied stress is a unique function of strain rate for a given structure [14]. Since the tensile flow stress was independent of strain the activation enthalpies were calculated from the tensile flow stress against temperature plots which are composites of the individual temperature and strain-rate change tests.

The calculated stress exponents, n, plotted against $\ln \dot{\epsilon}$ for c-axis sapphire are shown at constant temperatures in Fig. 5. The stress exponents, n, increase in value from about 4 at low strain rates to about 10 at high strain rates. These n values are inconsistent with all models of glide-rate controlled by climb which predict stress exponents in the range of 3 to 5 [15]. These n values are also inconsistent with the Weertman modified pure-climb diffusional mechanism [16] proposed as rate controlling for the creep of sapphire via pyramidal slip by Firestone and Heuer [6]. Their conclusions are based on data collected at high temperatures (1600 to 1800° C) and low strain rates (10^{-8} to 10^{-6} sec^{-1}) and stresses (70 to 114 MN m^{-2}). The calculated stress exponents in Fig. 5 seem to approach a value of 3 for the higher temperature data at lower strain rates.

The tensile flow stress against activation volume data are plotted for constant strain rates in Fig. 6. Note that at high stresses the activation volumes fall in a distinct band for all strain rates. At lower stresses the activation volumes tend toward smaller values. These smaller values correspond to the flow data at temperatures above the break in the constant strain-rate curves. Since the activation volume at high tensile flow stresses (lower temperature data) is about $10b^3$ (where $b = 0.512$ nm) this tends to support the idea of a Peierls process as rate controlling. The smaller activation volume at lower tensile flow stresses (higher temperature data) is consistent with expectations for a diffusion-controlled process.

The tensile flow stress against activation enthalpy data (see Fig. 7) indicates that at higher tensile flow stresses and strain rates the data fall on straight lines which can be extended to zero tensile flow stress to estimate values of H_0, the zero stress-activation enthalpy, of 130 to 150 kcal mol^{-1}.

At lower tensile flow stresses the apparent activation enthalpies are erratic and tend toward very

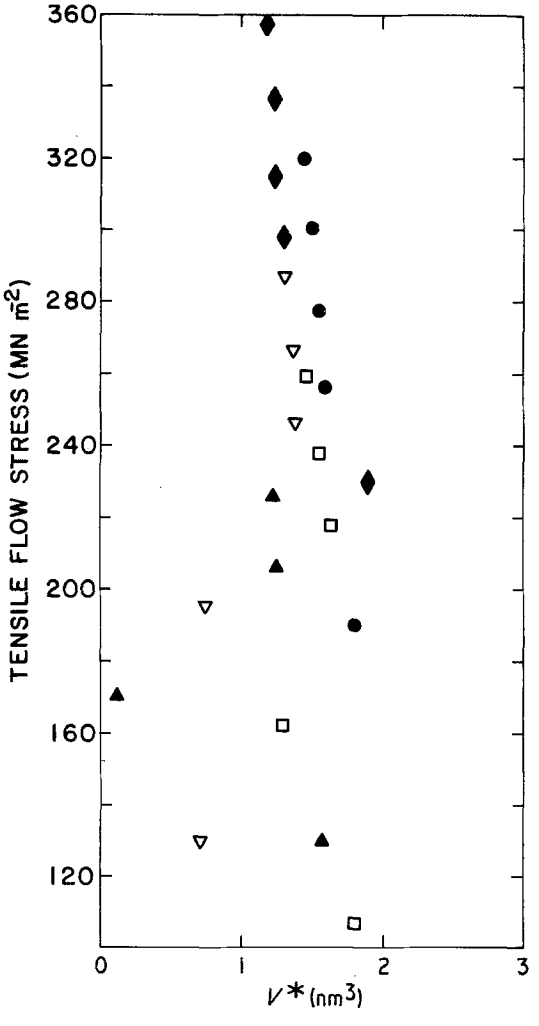

Figure 6 Tensile flow stress plotted against activation volume at constant strain rates for undoped c-axis sapphire. ○, 0.0036 min^{-1}; ♦, 0.0019 min^{-1}; ●, 0.00 73 min^{-1}; ▽, 0.000 36 min^{-1}; □, 0.000 19 min^{-1}; ▲, 0.000 07 min^{-1}.

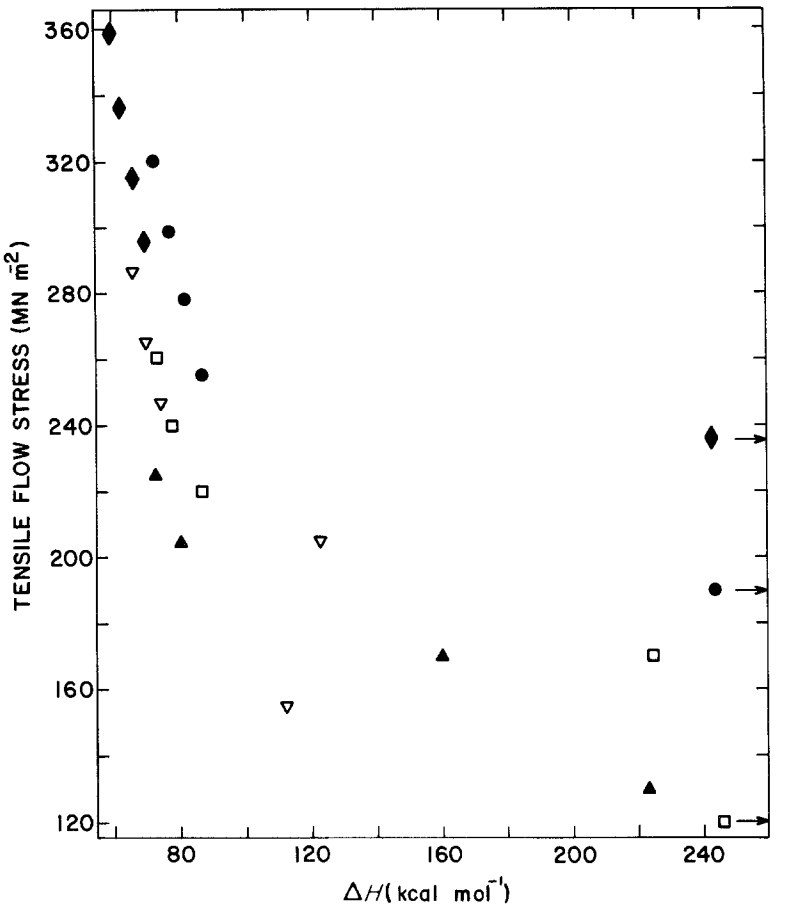

Figure 7 Tensile flow stress plotted against activation enthalpy at constant strain rates for undoped *c*-axis sapphire. ○, 0.0036 min^{-1}; ♦, 0.0019 min^{-1}; ●, 0.000 73 min^{-1}; ▽, 0.000 36 min^{-1}; □, 0.000 19 min^{-1}; ▲, 0.000 07 min^{-1}.

large values. These values are calculated from data in the higher temperature region beyond the break in the flow curves, and may be associated with a change in the rate-controlling process.

The rate-limiting process for plastic deformation of undoped *c*-axis sapphire at temperatures and strain rates above the break in the tensile flow stress curves requires further analysis. The deformation does not seem to be diffusion-controlled in this region since the stress exponents are variable and the activation enthalpies are very large. A simple Peierls process does not seem to be applicable since the activation volume tends towards small values ($< 10\,b^3$) and the activation enthalpies tend toward very large values. If the Peierls process is still rate-controlling in this higher temperature region there must be some modification of the basic Peierls process.

The temperature dependence of the Peierls barrier has been the subject of several studies [17]. In a review of these models Kuhlmann-Wilsdorf [18] noted that the predicted frictional stress acting on dislocations was substantially higher than that observed. For example, dislocations in close-packed metals move at very much lower stress levels than those calculated. In the past, several explanations have been given for such processes, including that of thermal activation. Kuhlmann-Wilsdorf considered the previously overlooked phenomena of the uncertainty relationship for dislocations in which the atoms that make up the dislocation are not considered as mathematical points since they vibrate and their positions do not ideally conform to the pattern of a dislocation with a precisely defined axis. The derived Kuhlmann-Wilsdorf [18] model for salts of the NaCl-type and b c c metals describes the temperature dependence of the Peierls stress when associated with the uncertainty in the position of the dislocation core caused by thermal vibrations and takes the form

$$\sigma = b \exp\left[-a(T/T_{mp})\right], \qquad (7)$$

where b and a are constants. Plots of homologous temperature, T/T_{mp}, against ln (flow stress) for experimental data at all strain rates in the higher

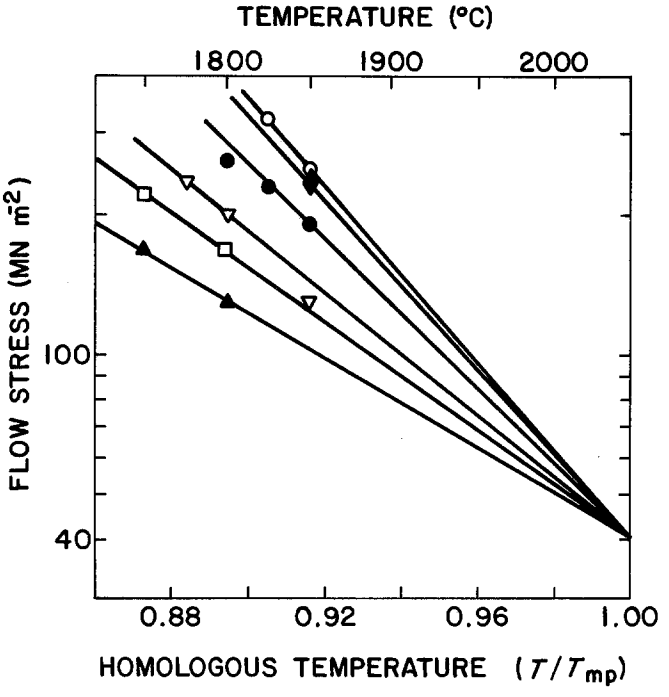

Figure 8 Flow stress in the high-temperature region plotted against homologous temperature at constant strain rates and high temperatures for undoped *c*-axis sapphire. ○, 0.0036 min^{-1}; ♦, 0.0019 min^{-1}; ●, 0.000 73 min^{-1}; ▽, 0.000 36 min^{-1}; □, 0.000 19 min^{-1}; ▲, 0.000 07 min^{-1}.

temperature region (see Fig. 8) fit this relationship and give a value (by extrapolation) for σ of 40 MN m^{-2} at the melting point. From this value and the data in Fig. 8 the constants a and b were determined for each strain rate. The equation of the form derived from the Kuhlmann-Wilsdorf model which fits the experimental data from the present study for the flow of *c*-axis sapphire in the high-temperature region is

$$\sigma = \exp 3[\ln \dot{\epsilon} + 14.37 - (\ln \dot{\epsilon} + 13.15)(T/T_{mp})]. \quad (8)$$

Higher temperature data are needed to substantiate the predicted curves even though the experimentally observed flow stresses show a good fit.

3.3. Microscopic analysis of deformed specimens

Fig. 9 is a SEM micrograph which shows the characteristic slip traces on a deformed *c*-axis filament. This observation is consistent with slip on either the $[1\,0\,\bar{1}\,1]$ plane (~18°) or the $[2\,2\,\bar{4}\,3]$ plane (~16°). Slip traces were not found on the filament outside the hot-zone length.

In order to establish the slip plane with more certainty, TEM methods were employed. It was found that at 100 kV the numbers and lengths of visible dislocation segments were insufficient to enable the slip plane to be identified. Stereo HVTEM microscopy at 1 MV was therefore undertaken. In practice great difficulties were experienced in achieving the optimum angle of tilt for maximum stereoscopic effect and in setting up identical diffraction conditions, principally because intense elastic strains in the thinned filaments produced numerous bend extinction contours. These difficulties, coupled with the fact that incipient climb effects in sapphire deformed at high temperatures reduce the definition of slip planes, meant that several sets of stereo pairs were necessary for the slip plane to be identified with certainty. There was close agreement between the orientations of the slip traces deduced from each stereo pair and one detailed analysis is illustrated

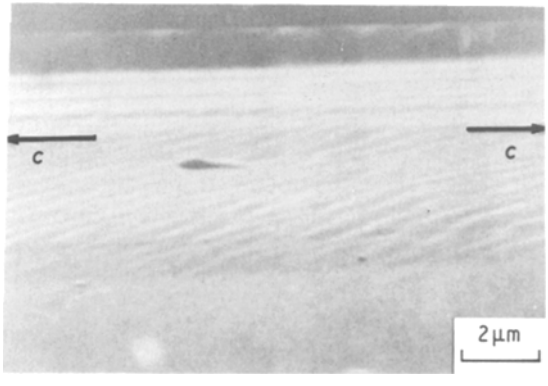

Figure 9 The characteristic pyramidal plane slip traces at approximately 18° to the *c*-axis.

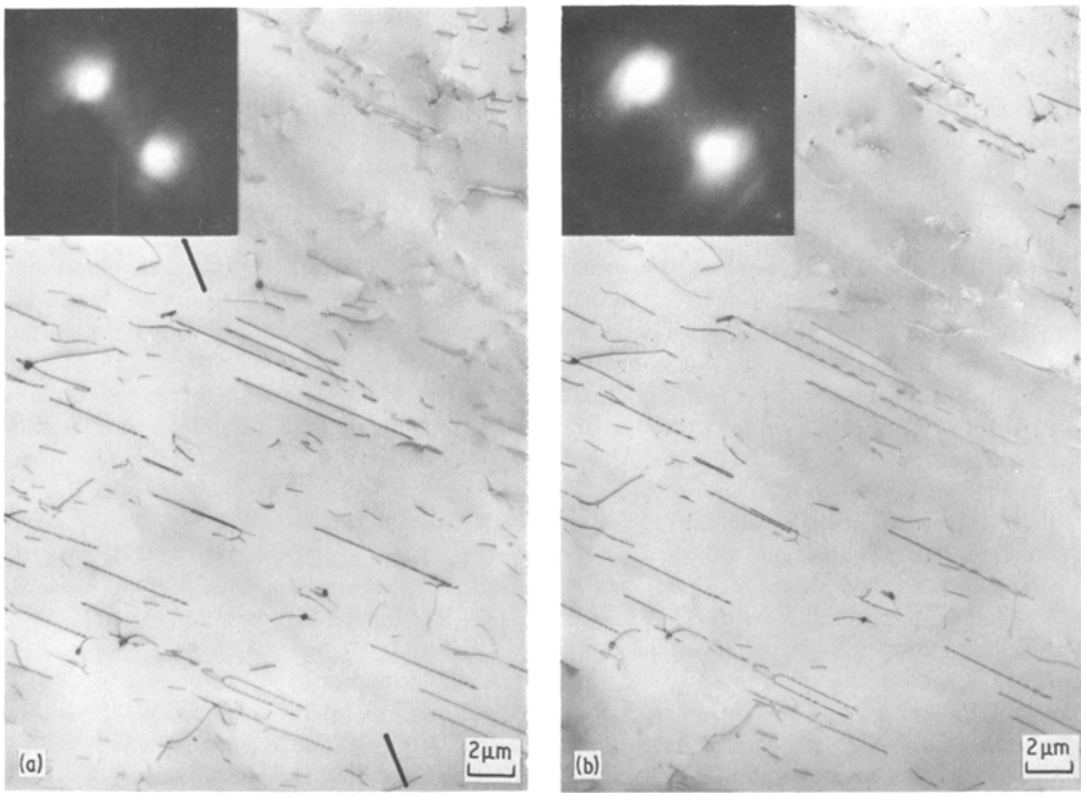

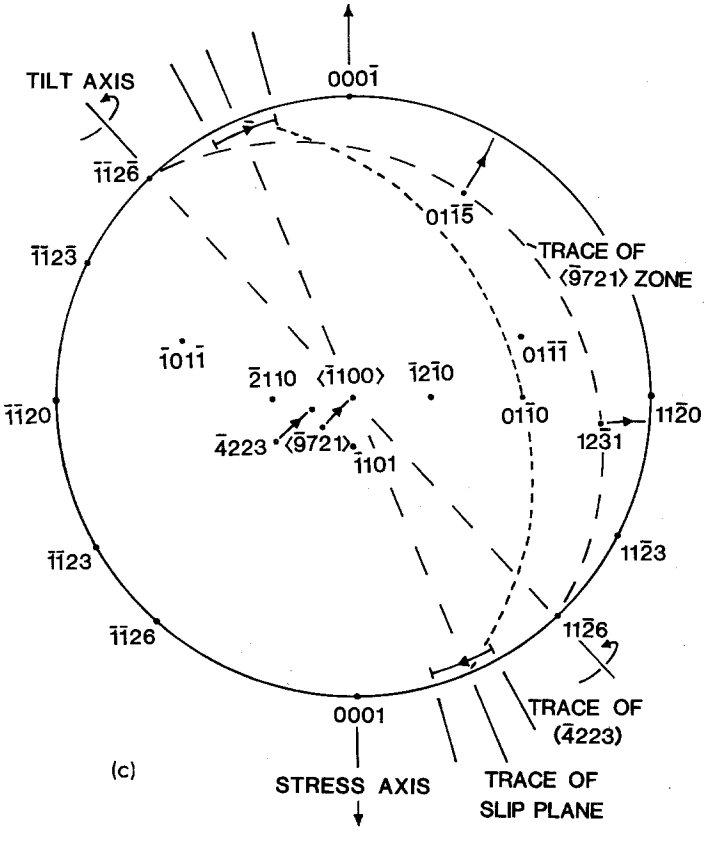

Figure 10 (a and b) Stereo-pair of slip dislocations in specimen deformed at 1850° C to 2% plastic strain at a strain rate of 0.007 min^{-1}, (stereo tilt angle ~ 12°) with g = $1\,1\,\bar{2}\,6$. The electron beam is approximately along a $[\bar{9}\,7\,2\,1]$ zone axis and a $[\bar{1}\,1\,0\,0]$ zone axis in Fig. 10a and b, respectively. (c) Stereographic projection corresponding to Fig. 10a and b, showing disposition of slip trace, tilt axis, possible $\{10\bar{1}1\}$ slip planes and poles of diffracting planes.

in Fig. 10a, b and c for a specimen deformed at 1850° C to about 2% plastic strain at a strain rate of $0.0007\,min^{-1}$.

The change in the angle of specimen tilt between the images in Fig. 10a and b is 12°, which gives only a weak stereo effect. In Fig. 10a the electron beam is parallel to a $[\bar{9}\,7\,2\,1]$ zone axis; in Fig. 10b the electron beam is approximately parallel to $[\bar{1}\,1\,0\,0]$, the two zones being 16° apart. The trace of the slip-plane deduced from this pair of images and the position of the tilt axis are shown in the stereographic projection shown in Fig. 10c, in relation to the pyramidal slip planes $\{1\,0\,\bar{1}\,1\}$. Cursory inspection suggests that the slip in this case involves the $(0\,\bar{1}\,1\,1)$ plane, whose trace in Fig. 10c corresponds to the trace of the slip plane deduced from Fig. 10a and b, to within experimental error. However, the projected widths of the slip planes in the images (3.9 to 3.5 μm in Fig. 10a and b, respectively) exclude $(0\,\bar{1}\,1\,1)$ as the slip plane, since this assignation would imply a HVTEM specimen thickness of $\simeq 10\,\mu m$. The actual foil thickness of $\simeq 1.5\,\mu m$ indicates that the normal to the slip plane must be inclined at about 22° to the electron beam. Further consideration suggests that the only possible slip plane consistent with the data is $(\bar{4}\,2\,2\,3)$, the poles of which are shown in Fig. 10c for the two stereo tilt angles. This conclusion is supported by the close agreement between the ratio of the projected widths of the slip planes (~ 1.05) and the ratio of the cosines (1:1) of the angle between the electron-beam direction and the pole of $(\bar{4}\,2\,2\,3)$ as it moves (from about 32 to 21°) during tilt.

An unequivocal determination of the corresponding slip direction has not been possible. The direction $[0\,1\,\bar{1}\,0]$ lies in the $(\bar{4}\,2\,2\,3)$ plane and on atomistic arguments it would be the most probable slip direction. The direction of elongation of most of the dipoles and pinched-off loops in the specimens is approximately $[0\,1\,\bar{1}\,0]$, but some doubt remains. Convincing diffraction contrast experiments to determine the Burgers vectors of dislocations could not be carried out, because of the frequent excitation of systematic and multiple electron reflections when operating at voltages between 400 kV and 1 MV, and because of the problems with bend contours in regions of the specimen which were transparent to 100 keV electrons.

The deduced slip plane and possible slip direction, $\{\bar{4}\,2\,2\,3\}\langle 0\,\bar{1}\,1\,0\rangle$ are consistent with the results of earlier work by Klassen-Neklyndova *et al.* [19]. The result raises questions as to why $\{1\,0\,\bar{1}\,1\}$ slip was not activated in the ideally-oriented *c*-axis filaments and whether the $1/3\langle 1\,0\,\bar{1}\,1\rangle$ Burgers vectors reported by Gooch and Groves [3] result principally from dislocation interactions.

4. Conclusions

Plastic strains of 3 to 5 per cent were observed for *c*-axis sapphire filaments deformed in uniaxial tension at 1600 to 1850° C with applied strain rates of 0.0007 to $0.0036\,min^{-1}$. The dislocation structures of the deformed specimens contained loops, dipoles, and straight glide dislocations. The slip traces and HVTEM stereo images provide evidence for the $\{\bar{4}\,2\,2\,3\}$ slip plane with the most likely direction being $\langle 0\,\bar{1}\,1\,0\rangle$.

The activation analysis of the flow data suggests that the rate-controlling process is the thermally-activated overcoming of the Peierls barrier.

Acknowledgements

The authors gratefully acknowledge the support of the National Science Foundation, Division of Materials Research; and the assistance of Dr J. F. Humphreys, Imperial College, London, in the use of the HVTEM.

References

1. J. B. WACHTMAN, Jr, and L. H. MAXWELL, *J. Amer. Ceram. Soc.* **40** (1957) 377.
2. M. V. KLASSEN-NEKLYUDOVA, *Zh. Tekh. Fiz.* **12** (1942) 519, 535.
3. D. J. GOOCH and G. W. GROVES, *J. Mater. Sci.* **8** (1973) 1238.
4. R. E. TRESSLER and D. J. BARBER, *J. Amer. Ceram. Soc.* **57** (1974) 13.
5. A. H. HEUER, R. F. FIRESTONE, J. D. SNOW and J. TULLIS, in Proceedings of the Conference on Ceramics in Severe Environments, Raleigh, NC, December 1970 (Plenum Press, New York 1970) p. 331.
6. R. F. FIRESTONE and A. H. HEUER, *J. Amer. Ceram. Soc.* **59** (1976) 24.
7. D. J. MICHAEL and R. E. TRESSLER, *J. Mater. Sci.* **9** (1974) 1781.
8. J. S. HAGGERTY, Air Force Materials Laboratory Technical Report number AFML-TR-73-2 (1973).
9. R. E. TRESSLER and R. L. CRANE, in "Advanced Materials: Composites and Carbon", American Ceramic Society Symposium, Chicago, IL, April 1971 (American Ceramic Society, Columbus, Ohio, 1971) p. 59.
10. H. CONRAD, *J. Amer. Ceram. Soc.* **48** (1965) 195.
11. H. CONRAD, G. STONE and K. JANOWSKI, *Trans. AIME* **233** (1965) 889.

12. B. L. BERTOLOTTI and W. D. SCOTT, *J. Amer. Ceram. Soc.* **54** (1971) 286.
13. R. CHANG, *J. Appl. Phys.* **31** (1960) 484.
14. A. G. EVANS and R. D. RAWLINGS, *Phys. Stat. Sol.* **39** (1969) 9.
15. T. G. LANGDON, in "Deformation of Ceramic Materials" edited by R. C. Bradt and R. E. Tressler (Plenum Press, New York, 1975) p. 101.
16. J. WEERTMAN, *ASM Trans. Q.* **61** (1968) 681.
17. J. P. HIRTH and J. LOTHE, "Theory of Dislocations" (McGraw-Hill Book Co., New York, 1968).
18. D. KUHLMANN-WILSDORF, *Phys. Rev.* **120** (1960) 773.
19. M. V. KLASSEN-NEKLYUDOVA, V. G. GOVERKOV, A. A. UMSOVSKAYA, N. N. VOINOVA and E. P. KOZLOVSKAYA, *Phys. Stat. Sol.* **39** (1970) 679.

Received 28 October
and accepted 16 November 1981